Electrochimica Acta 299 (2019) 1011–1023

Contents lists available at ScienceDirect

Electrochimica Acta

journal homepage: www.elsevier.com/locate/electacta

Electrochemical solid-state nanosensor based on a dual amplification strategy for sensitive detection of (Fe^{III}-dopamine)

Sepehr Lajevardi Esfahani [a], Shohre Rouhani [a, c, *], Zahra Ranjbar [b, c]

[a] Organic Colorants Department, Institute for Color Science and Technology (ICST), Tehran, Iran
[b] Surface Coatings and Novel Technologies, Institute for Color Science and Technology (ICST), Tehran, Iran
[c] Center of Excellence for Color Science and Technologies, Institute for Color Science and Technology (CECST), Tehran, Iran

ARTICLE INFO

Article history:
Received 30 October 2018
Received in revised form
8 January 2019
Accepted 10 January 2019
Available online 11 January 2019

Keywords:
Dopamine
Layer-by-layer (LbL) assembly
Solid-state
Electro-active naphthalimide
LDH

ABSTRACT

Over the past decades, according to empirical studies, it has been determined that dopamine metabolism plays a key role in many neuropsychiatric diseases. The development of dual-response electrochemical sensors is still in its infancy during the sensor-based detection methods for dopamine. Hence, a novel electrochemical sensor with dual amplification strategy was designed and constructed. In the molecular design of the solid-state structure, a flexible ITO/PET was used. Several nanometric layers of graphene oxide (GO) were deposited on the surface of the ITO/PET using the electrophoretic deposition (EPD) method. Then, during the layer-by-layer (LbL) assembly, the synthesized electro-active naphthalimide dye/LDH nanoplatelets matrix (NALD-n) was displayed in successive layers. The minimum sheet resistance, uniform morphology, and high electrocatalytic activity of the modified matrix film were obtained in the fifth cycle of the LbL assembled (NALD-5) modified electrode. This molecular design resulted in a significant increase in the fluorescence emission of electro-active dye in the sensor's bed containing LDH nanoplatelets and eliminating the effect of GO quenching. This solid sensor was used to detect dual Fe^{3+}/dopamine through an electro-active naphthalimide probe on the surface. In this sensor, in terms of electrochemical/optical changes of solid-state, the (OFF/ON/OFF) system was created so that the fluorescence emission decreased with the presence of dopamine molecules. The cyclic voltammetric changes of the sensor were well tolerated at a linear range of [1.0×10^{-10}-1.5×10^{-8} M] for the selective sensing of dopamine with a detection limit (LOD) of 0.06 nM.

1. Introduction

The basis of electrochemical sensors with dual amplification strategy (electrochemical/optical) is the measurement of the signal by electrochemical and optical methods simultaneously. The advantages of this kind of sensor are its high sensitivity, broad dynamic range, and low background, ease of use, high flexibility, and extraordinary biological applications [1–3]. In general, electro-optical devices based on multi-layer composites have better performance and optical efficiency than single-layer-based equipment [4]. Multi-layer composites are limited in terms of stability and the ability to reproduce them. One possible solution to achieving even greater uniformity and performance of nanoscale composites is through layer-by-layer assembly (LbL) [5,6]. The thin films accumulated in the LbL method are prepared by the sequential adsorption of several large molecule components, such that strong gravitational forces such as electrostatic interactions, hydrogen bonding, van der Waals interactions, and load transfer complexes are established between the layers. Applications of two-dimensional nanocomposites based on the LbL method include thin films with special electronic properties, carbon materials, energy storage media, and bio-applications [7]. Dopamine (DA) is one of the cathecholamine neurotransmitters of the central nervous system in the human brain; it plays an important role in the brain functions and emotional responses of humans. Excessive DA (e.g., Huntington's disease) reduces energy metabolism and ultimately leads to death. On the other hand, the deficiency of DA leads to a loss of muscle control and Parkinson's disease; therefore, the quantitative and accurate detection of DA levels is very important. Recently, various studies have been conducted to apply unique materials for developing biosensors for in vivo and ex vivo sensing

* Corresponding author. Organic Colorants Department, Institute for Color Science and Technology (ICST), Tehran, Iran.
E-mail address: rouhani@icrc.ac.ir (S. Rouhani).

https://doi.org/10.1016/j.electacta.2019.01.065
0013-4686/

of neurotransmitters. These materials include nanomaterials, polymers and biomolecules that are used in the structure of sensor equipment. For in vivo sensing, electrochemical techniques have been widely used, as a high-speed cyclic voltammetry (CV) method is the most widely used technique [8]. There are also other features such as the simple structure of the equipment and the high sensitivity of the advantages of this method. Neurotransmitters have been detected in various investigations are mainly DA, EP, NE, 5-HT, Glu, His, tryptamine, and ACH. Table 1 lists the main characteristics of the sensors made in various studies for the detection of DA.

Among the measurement methods, the fluorescence technique is a simple, low-cost, and precise technique, but its accuracy is not so high for DA detection in real samples. The concentration of DA in living systems is very low (in the range of 26–40 nM or less) [36,37]. Therefore, a method that is both easy to use, cost effective, and has higher accuracy than the pure fluorescence method is of great interest. In this research work, the molecular design of a solid-state electrochemical sensor that exhibits both electrochemical behaviour in the presence of the target molecule and its fluorescence emission changes with/without target molecules has increased the accuracy of detecting target molecules. Its ease of use and high precision make it more attractive to biologists. Layered double hydroxides (LDHs) are two-dimensional compounds of the general type of anion clay that are widely used in optical, biological, and electronic applications [38–41]. The chemical structure of LDHs can be introduced as $[M^{II}_{1-x}M^{III}_{x}\ (OH)_2]^{-}(A^{n-})_{x/n}.\ mH_2O$ (M^{II} and M^{III} are divalent and trivalent metals, respectively, and A^{n-} is an inter-layered anion) [38]. Due to the two-dimensional structure, the flexibility and ionic exchange of LDHs, and with the help of the layer-by-layer (LbL) assembly method, they have been combined with a suitable organic molecule in a regular-layered arrangement with each other and has formed organic/inorganic compounds that are widely used in various fields of science [42,43]. The use of LDH nanoplatelets and structural reforms on their surface has found widespread use in the development of electronic and optoelectronic devices [44]. Graphene with its unique electrical, optical, and mechanical properties has been used in many aspects of electronic equipment such as electrochemical sensors with high detection speed [45,46]. Many studies have shown that graphene compounds are one of the most important quencher substances [47–49]. Therefore, the position of these compounds in the design of a solid-state sensor is because of their high electrical conductivity, and the challenge is because of the effect of quenching by placement next to a fluorophore. In this research work, a novel electrochemical sensor with dual amplification strategy was designed and constructed. The main element of the sensor electrode consists of ITO/PET, which is coated by the EPD method with GO with a thickness of several nanometers. This very conductive electrode is layered by means of the LbL method to form an interconnected matrix of Mg–Al LDHs/electro-active naphthalimide dye to reach an optimized cycle for optimal electro-optical properties of the modified electrode. This dual electrode was then used to detect Fe^{3+} and, due to its ability to form a strong chelate between Fe^{3+} and DA, to detect very low amounts of DA by means of Fe^{3+} intermediates.

2. Experimental

2.1. Materials

The materials used in the GO electrodeposition section (with their suppliers) include graphene oxide nanoplatelets of analytical grade [50] (Nanosany Co.), $Mg(NO_3)_2$, NaOH, methoxy-ethanol (Merck Co.), and ITO/PET sheet (60 Ω cm^{-1}, Sigma Aldrich Co.).

Ferrocenecarboxaldehyde, hydroxylamine, lithium aluminium hydride, 3,4-dihydroxyphenethylamine (dopamine), L-ascorbic acid (AA), 2,6,8-trihydroxypurine (uric acid/UA), triethylamine, iron (III) sulfate hydrate, acetate buffers, and phosphate buffer solution 0.1 M (PBS) were obtained from Sigma Aldrich Co. Dimethylformamide (DMF), ethanol, petroleum ether, diethyl ether, dichloromethane (CH_2Cl_2), tetrahydrofuran (THF), acetone, and

Table 1
The main characteristics of DA detection sensors developed in various studies.

Sensor based on	Materials Used	Measurement Technique	LOD	Reference
Carbon materials	Graphene, Carbon fiber	DPV	1.36 μM	[9]
Carbon materials	Reduced graphene oxide	DPV	1.4 μM	[10]
Carbon materials	Carbon dots	DPV	10 nM	[11]
Carbon materials	Graphene oxide, MWCNT	DPV	1.5 μM	[12]
Carbon materials	Reduced graphene oxide, MWCNT	ECL	0.067 μM	[13]
Carbon materials	Graphene oxide	Amperometry	0.277 μM	[14]
Carbon materials	Nafion-coated MWNT yarn	DPV	0.01 μM	[15]
Carbon materials	Fluorescent single-walled carbon nanotube	Near-IR fluorescence	11 nM	[16,17]
Carbon materials	Graphene quantum dots	Fluorescence	22 nM	[18]
Carbon materials	High quantum yield sulphur doped carbon dots	Fluorescence	47 pM	[19]
Polymer	Overoxidized polypyrrole	Amperometry	62 nM	[20]
Polymer	Graphene/polypyrrole	Amperometry	2.3 μM	[21]
Polymer	Poly (hydroquinone)	DPV	41.9 nM	[22]
Polymer	Poly (2,4,6-triaminopyrmidine)	DPV	0.017 μM	[23]
MIP	Poly (o-aminophenol)	DPV	1.98 nM	[24]
MIP	Polypyrrole	DPV	10 nM	[25]
MIP	Polypyrrole	DPV	33 nM	[26]
MIP	Poly (nicotinamide)	CV	8 nM	[27]
Biomolecule	Aptamer	DPV	10 nM	[28]
Biomolecule	Aptamer	DPV	0.22 nM	[29]
Biomolecule	Aptamer	Amperometry	1.8 nM	[30]
Biomolecule	Aptamer	DPV	700 ± 19.23 pM	[31]
Biomolecule	Aptamer	DPV	78 fM	[32]
Nanomaterial	Green synthesized silver nanoparticles	UV–vis.	0.2 μM	[33]
Nanomaterial	Gold nanorods	Colorimetric	1 μg mL^{-1}	[34]
–	Optical neurotransmitter sensor (MWONS)	Near-IR fluorescence	100 nM	[35]

isopropyl alcohol were purchased from Merck Chemical Co. All solvents were of analytical grade.

2.2. Apparatus

The electrophoretic deposition process of the GO suspension was done through a Zahner potentiostat (PP-200/England). The oven (Carbolite/CSF1100/England) was used for thermal annealing of the prepared samples. Absorption measurements were made with a single beam UV–vis spectrophotometer (CECIL CE9200/England) from 200 nm to 800 nm. The sheet resistance of modified electrodes was measured with Fluke Ohmmeter (1550B/USA). Scanning electron microscopy (SEM) and atomic force microscopy (AFM) tests were used to evaluate the prepared samples using (LEO 1455VP/Germany) and (Micro Photonics Inc/Dual scope DS95-200E/USA) instruments, respectively. A fluorescence spectrometer (Perkin-Elmer LS55/USA) was used to measure the fluorescence intensity of the tested samples. To test the electrocatalytic function of the prepared electrodes, cyclic voltammetry (CV) was performed on electrodes using a (Zahner PP211 potentiostat/England) in a three-electrode electrochemical cell. In this test, the surfaces of the prepared electrodes were used as the working electrodes, platinum was used as the counter electrode, and Ag/AgCl was used as the reference electrode. A PBS solution (0.1 M in deionized water/pH = 7.0) was used as the standard electrolyte in CV tests. In all CV tests, the scan potential step was 0.005 V, and the potential scanning speed was 0.05 Vs^{-1}.

2.3. Methods

First, the stable suspension of 0.01 (%w/w) GO in distilled water was prepared through the ultra-sonication process (@ 35 Hz/40 °C for 2 h) [50]. Under these conditions, the suspension was completely stable for 6 months, and the pH of the suspension was 2.7 at 23 °C. The stable GO suspension was then mixed with 4 mL of methoxy-ethanol and 0.5 mL of 5% (w/w) NaOH in distilled water. Under these conditions, the pH of the stable suspension was 7.7. Therefore, the GO suspension was suitable for anodic electrophoretic deposition.

2.4. Electrophoretic deposition process

For the anodic electrophoretic deposition process of the GO suspension, the ITO/PET (6 × 30 mm diameters and treated with isopropyl alcohol) and graphite rod were used as anode and cathode, respectively. The distance between the anode and the cathode was 5.0 cm, and the anode-to-cathode area ratio was 3.3. The temperature of the electrophoretic bath was kept at 25 °C for all of the samples.

The electrophoretic conditions of GO deposition on ITO/PET (GO concentration, application potential, application time, and thermal annealing conditions) were 0.01% w/w, 2 V, 10 s, and 1 min @ 100 °C, respectively [50].

2.4.1. Synthesis of N-ferrocenyl-1,8-naphthalimide (FC-NAPH)

N-ferrocenyl-1, 8-naphthalimide was prepared according to a two-step literature procedure [51] (see Schemes 1 and 2).

2.4.2. Fabrication of the NALDs film modified electrode

Mg–Al LDHs (including nitrate anion) was synthesized using the method developed by the ICRC Research Group [52]. The colloidal suspension of Mg–Al LDHs nanoplatelets in deionized water (1.0 g L^{-1}) was prepared under ultra-sonication in a sonicator bath (Bandelin electronic/510 h) at 40 °C for 4 h.

To investigate the effect of pH on adsorption of LDH nanoplatelets and FC-NAPH dye molecules on the electrode surface in a range of pH values (3.5–11.5), LDH suspension was adjusted by different pH buffers (acetate/carbonate). The GO/ITO/PET electrode was immersed in LDH suspension for 10 min. The electrode was then removed and rinsed with distilled water. Then it was immersed in FC-NAPH solution in DMF (1.0 g L^{-1}). After immersion of electrode in FC-NAPH solution, rinsing and drying the electrode (with a nitrogen gas flow for 2 min at 25 °C), UV–vis spectroscopy test was taken from the electrode surface. A series of these operations for LDHs nanoplatelets and FC-NAPH were repeated n times to obtain multilayer films of (NALD-n).

Scheme 1. Synthesize reaction of *N*- Ferrocenylmethylamine.

Scheme 2. Synthesize reaction of *N*-ferrocenyl-1,8-naphthalimide.

3. Results and discussion

3.1. Characterization of electrodeposited films on electrode

According to the structural model of GO (introduced by Gao et al. [53]), the most functional groups of GO are hydroxyl (OH), carboxylic acid (COOH), and epoxy (COC); by stable suspension of GO in water and surface ionization of functional groups, the effective surface charge of this compound is negative [50]. In the electrical field of the EPD process, GO is attracted to the positively charged surface (anode). Within 10 s of applying electrical potential, the changes in the electric current at very low speeds and the slope have bullish trends, indicating the conductivity of the initial surface and the conductivity consistency of the surface to the tenth of a second. The very low current density (averaging about 0.014 mA cm^{-2}) indicates a very low thickness of deposited GO on the surface of the electrode.

The scanning electron microscopic images of uncoated ITO/PET electrode, the ITO/PET electrode coated with GO (GO/ITO/PET), and the (NALD-5) electrode are shown in Fig. 1.

Fig. 1a shows the morphology of the surface of the (ITO/PET) electrode without any surface modification; the coated indium tin oxide particles on the PET surface are characterized by a pattern of small white particles. In Fig. 1b, the presence of a very thin and wrinkled GO layer that continuously covers the entire surface of the (ITO/PET) electrode is shown. In Fig. 1c, the matrix of the LDH nanoplatelets is identified along with the dye matter that is continuously adsorbed on the surface of the (GO/ITO/PET) electrode by a pattern of layer-by-layer accumulation.

The results of sheet resistance measured in different electrodes prepared in different LbL cycles (n) are shown in Fig. 2.

As can be seen, the sheet resistance was reduced by about 24 Ω with the EPD of GO on the surface of the (ITO/PET) electrode, due to

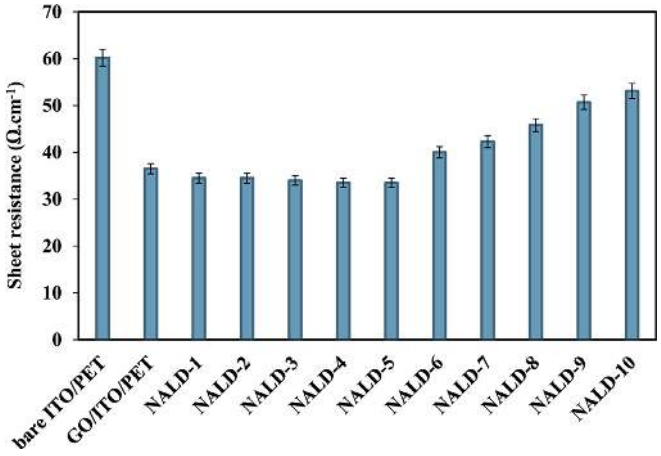

Fig. 2. Sheet resistance changes of prepared electrodes.

obtaining the least sheet resistance (the highest electrical conductivity) of the modified electrode.

3.2. Characterization of LbL assembly of $(NALDs)_n$ matrix film-based electrodes

To obtain the optimum conditions for adsorption of LDH nanoplatelets on the solid-state electrode, the effect of LDH suspension pH was investigated. UV–vis spectrophotometry method was used for this. Because the LDH in the [260–360] region have index absorption peaks [54]. The results of the pH optimization for LDH colloidal suspension are shown in Fig. 3.

Because the ionic conditions of the FC-NAPH solution were constant, the difference between the adsorption of LDH nanoplatelets and that of FC-NAPH can be explained by the difference in pH of the LDH colloidal suspension. As the results show, the maximum adsorption of LDH nanoplatelets with FC-NAPH molecules after five LbL cycles was observed in pH 5.5. Due to the isomeric displacement phenomenon in a LDH crystal network (replacing Mg^{2+} instead of Al^{3+}) and the charge level dependent on the pH caused by the protonation/deprotonation on the LDH surface, metal ions of LDH are dissolved in very acidic conditions ($pH < 4$) and the structure of the LDH is changed. The dissolution of LDH is not observed in other pH values [55–57]. The point of zero charge (PZC) is said to be the pH at which the opposite charges are

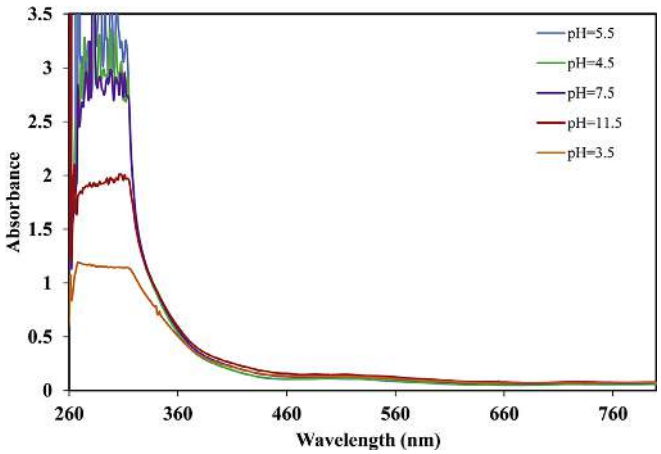

Fig. 3. Absorbance changes of NALD-5 against pH of LDH colloidal suspension (1 g L^{-1}) in deionized water.

Fig. 1. SEM images of (a) uncoated ITO/PET, (b) GO/ITO/PET and (c) NALD-5 electrode.

an increase in the electrical conductivity of the electrode surface with the GO electrically deposited (a multi-nanometer thickness) on the electrode surface. With the (NALDs) matrix layer-by-layer assembly on the electrode surface until the fifth cycle, there is no significant change in the sheet resistance (or electrical conductivity) of the electrode. From the fifth cycle, increasing the density of the LDHs nanoplatelets along with the dye matter, due to the increased length of the electron transfer pathway, causes an increase in the sheet resistance of the electrode. Therefore, the fifth cycle of the LbL assembly is considered as the optimum cycle for

zero under constant temperature, pressure, and medium. Research has shown that PZC exists for LDHs [56]. In a study by Sepehr et al. [54], the PZC of LDH suspension is measured that was equal to 5.5. They determined that dye adsorption behaviour on LDH surfaces (based on ionic structure of the dye) is highly dependent on the LDH suspension pH and the PZC, so that when the pH of the suspension is less than that of the PZC, the dominant charge of the LDH nanoplatelets is positive (due to the presence of Mg^{2+} and Al^{3+} ions in the basal surfaces of LDH), and in pH range more than the PZC, the dominant load of LDH nanoplatelets is negative (due to the deprotonation of the LDH and the concentration of hydroxyl groups at the edges of the LDH surfaces). Regarding the PZC measured in our research work, which is equal to 5.5, the maximum adsorption of LDH with synthetic dye (FC-NAPH) is considered at pH 5.5. Due to the structure of the synthetic dye that is nonionic and has fused rings in the naphthalimide structure, the dye adsorption on the surface of the LDH is mainly due to the van der Waals interactions and the formation of intermediate complexes between the layers of LDH surfaces and dye molecules. The adsorption of proton charge on the LDH surface can alter the pH of the medium. Moreover, due to the effect of electrostatic bonding in different pH conditions, the arrangement of LDH nanoplatelets (basal and prismatic surfaces) has different tendencies for the adsorption of dye molecules. According to the results, in severe acidic conditions (pH < 4), due to the dissolution of metal ions on the basal surface of the LDH, the amount of stable and unsolvable LDH nanoplatelets that are adsorbed on the solid electrode surface will be minimal. Otherwise, in a completely alkaline pH, LDH nanoplatelets may be flocculated due to the attractive interactions between the negatively charged edges and the positive charge of the basal surface, resulting in less permanent adsorption of LDH on the solid surface [55].

To determine the changes in the fluorescence emission, the initial surface of the (ITO/PET) electrode, and this electrode along with GO and in different cycles of the LbL assembly of $(NALDs)_n$ matrix on the electrode surface, spectrofluorimetry was performed on different electrodes. The results of the fluorescence emission of materials used before developing the electrochemical sensor are shown in Fig. 4.

As shown in the results of Fig. 4a, the (ITO/PET) electrode had a weak fluorescence emission at an excitation wavelength of 230 nm. When GO was deposited on the surface, the fluorescence emission was severely weakened, and GO, as a quencher, turned off the fluorescence emission of the electrode. The result of the spectrofluorometric test on the FC-NAPH solution (1.0 g L^{-1} in DMF) is shown in Fig. 4b. The maximum fluorescence emission of FC-NAPH solution at the excitation wavelength of 388 nm was about 350 units at 460 nm. On the other hand, the fluorescence emission for LDH suspension was not apparent on its own, but when the dye mixture and LDH suspension were obtained, increased fluorescence emission was evident (see Fig. 4b).

The fluorescence behaviour of the fluorescent dye along with the LDHs nanoplatelets should be checked when LbL assembly is done on the solid surface containing few GO layers (as a strong quencher), to determine whether the creation of a spacing in the (NALDs) matrix film results in a change in the fluorescence emission, and the GO quenching effect is depressed. For this purpose, the spectrofluorometric test of the modified electrodes was performed in different LbL cycles (n). The result of the spectrofluorometric test of the prepared electrodes is shown in Fig. 5a.

As is clear from the results shown in Fig. 5a, in the first to third LbL cycles, the fluorescence emission of the solid modified electrode surface was very low and less than 20 units. This is due to the less spatial space created in low LbL cycles. Based on the results of the topographic AFM test, the thickness of the created layers to the third cycle was about 25 nm. According to the measured energy levels of LUMO and HOMO of FC-NAPH fluorophore (Fig. 5b), which is approximately equal to −3 and −5.5 e (respectively), the energy level of GO was approximate −4.5 eV. No injection of the electron to the HOMO level of fluorophore caused the fluorescence quenching of the dye molecule. According to three-dimensional topographic AFM images obtained from each of the samples (Fig. 5c), it is clear that the increase in different layers adsorbed on the surface in the order of the layering steps resulted in increased thickness and increased surface roughness profile. As with the GO layer deposited on the electrode surface under EPD conditions, the uniform thickness of the few wrinkled GO layers with an average of 5.4 nm covered the surface of the (ITO/PET) electrode continuously. Also, with the $(NALDs)_n$ until the fifth cycle, the thickness of the adsorbed layers on the (GO/ITO/PET) surface in the fifth cycle reached about 140 nm. By increasing the number of LbL cycles and increasing the density of the molecules of FC-NAPH adsorbed alongside the LDH nanoplatelets in the matrix created on the solid surface and increasing the thickness of the adsorbed layers in the fourth and fifth cycles, there is a mutation to increase the fluorescence emission of the modified electrodes. LDHs placement along with fluorophore leads to the significant enhancement of the fluorescence emission of the fluorophore. The reason for this can be related to the separation of fluorophore molecules on the LDH surface [55]. The thickness of the LbL assembled $(NALDs)_5$ matrix

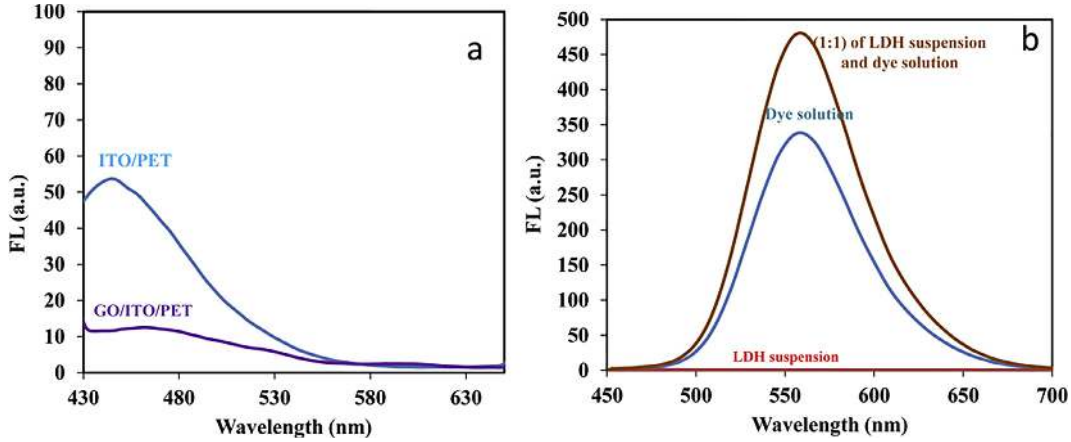

Fig. 4. (a)The fluorescence emission of ITO/PET compared to GO/ITO/PET (λexc. = 230 nm) in air environment, (b) comparison of fluorescence emission of (FC-NAPH) solution (1.0 g L^{-1} in DMF), LDH suspension (1.0 g L^{-1} in deionized water) and mixture of dye solution and LDH suspension (1.0 g L^{-1}).

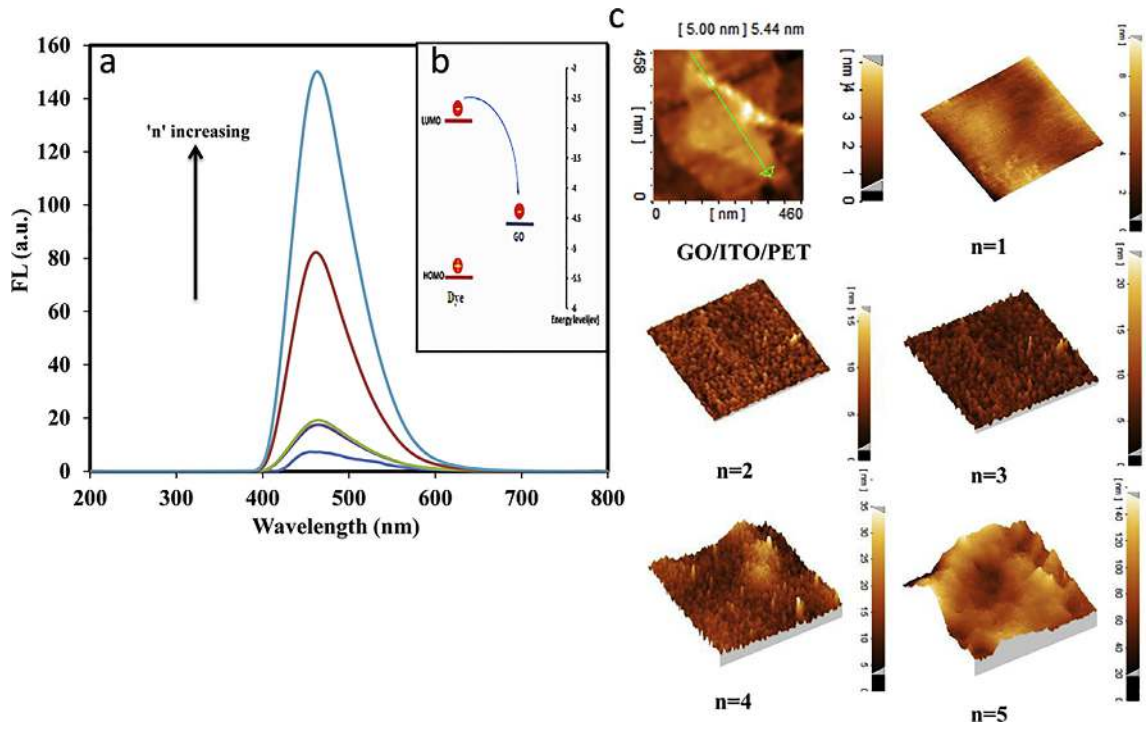

Fig. 5. (a) The fluorescence emission changes of modified electrodes in different LbL cycles (λexc. = 388 nm), (b) Comparison of calculated energy levels of FC-NAPH and GO, (c) 3D-topographic AFM images of GO/ITO/PET and LbL assembled of $(NALDs)_n$ on GO/ITO/PET.

reaches about 140 nm that excludes Förster resonance energy transfer (FRET) distance [58]. The results of this research are consistent with the FRET mechanism in solid-state electrodes.

3.3. Explaining sensor parameters

Because of the modified structure of the GO/ITO/PET electrode and the presence of a composite thin-film of the electro-active dye along with the Mg–Al LDH nanoplatelets, this flexible electrochemical electrode is an efficient sensor against the electro-active target molecules with appropriate conductivity and electrocatalytic properties and the emission of an acceptable amount of fluorescence. In this research, this electrode was used to detect very low Fe^{3+}/DA concentrations using the electrochemical CV technique and optical changes on the electrode surface using fluorimetry. The CV test results of the modified electrodes with and without the presence of different concentrations of Fe^{3+} ions are shown in Fig. 6.

Fig. 6a shows the cyclic voltammetric results of (ITO/PET) and (GO/ITO/PET) electrodes in neutral PBS electrolyte. As indicated in the graphs, due to the presence of very thin GO layers on the surface of the GO/ITO/PET electrode and the increase in surface conductivity, the electric current transferred from the electrode surface, and the width of the graph is larger than the peak associated with the uncoated ITO/PET electrode. However, in the range of −0.5 to 1.0 (V vs Ag/AgCl), the oxidation/reduction peaks are still unknown. With the $(NALD)_n$ matrix LbL assembly on the electrode surface and increasing the number of LbL cycles, the values of about −0.07 V (E_{pa}) and −0.315 V (E_{pc}) were determined in the (NALD-5) electrode for anodic and cathodic signals, respectively, which were related to the redox changes of the ferrocene compound bound to the structure of the synthetic dye (FC-NAPH) on the electrode surface in the PBS electrolyte. Viehbeck et al. [59] showed in their study that imide system structures (like 1, 8-naphthalimide) display two reversible redox couples. The first redox couple, $^1E^0$, involves the reduction of the neutral form to the radical-anion form, while the second redox couple, $^2E^0$, at a more negative potential, is the reduction to the dianion state. In their study and similar studies, the two potentials ($^1E^0$ and $^2E^0$) of 1,8-naphthalimide are −1.26 and −1.87 (V vs SCE), respectively. Therefore, with respect to the single-peak oxidation and reduction observed in the current research results and given the selected potential range, this peak index can be attributed to the electro-oxidation of ferrocene in the structure of FC-NAPH. The peak separation potential ($\Delta E_p = E_{pa}$-$E_{pc} = 245$ mV), is much greater than the expected one (59/n) mV for a reversible system. This suggests that NALD-5 exhibits a quasi-reversible behaviour in the PBS solution, and there will be a mediated electron transfer at the (NALD-5) electrode by ferrocene (Fc) [60–62]. Earlier reports on ferrocene-modified carbon paste electrodes (FMCPE) have also mentioned that FMCPE exhibits a diffusion controlled quasi-reversible behaviour [63]. As evidenced in cyclic voltammetric graphs, the intensity of the peak changes associated with the oxidation reaction carried out at the electrode surface (by varying the Fe^{3+} concentration) is less than the cathodic peak variation $\left(\left|\frac{I_a}{I_c}\right| = 0.404\right)$. The reactions involved at the electrode surface can be written as illustrated in Scheme 3.

By increasing the concentration of Fe^{3+} as an oxidation reagent, the reaction in Scheme 3 tends to the right and the fluorescence emission increases. On the other hand, when the Fe^{3+} concentration is increased, the $(Fc\text{-}naphthalimide)^+$ concentration is also increased, and this justifies the higher intensity of the cathodic current (i_{pc}) compared to the anodic current (i_{pa}) in the results obtained from the CV test.

The anodic and cathodic peak current changes enhance linearly along with the increase of Fe^{3+}concentration. The linear response ranges in [0.5×10^{-6}-8×10^{-5} M] with a detection limit of 0.03 μM for Fe^{3+} was obtained.

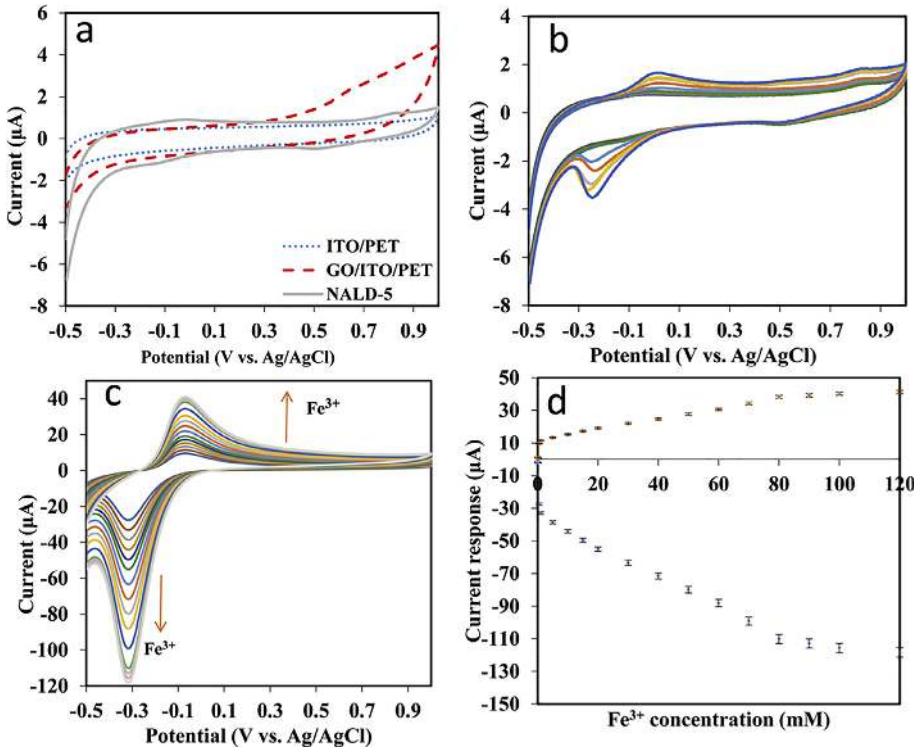

Fig. 6. The cyclic voltammograms of (a) NALD-5 compared to ITO/PET and GO/ITO/PET, (b) NALD-5 electrode in PBS solution including different Fe^{3+}concentrations in range of [0.5–200 μM], (c) NALD-5 electrode in PBS solution including different Fe^{3+}concentrations in range of [1–120 mM], (d) current response of NALD-5 electrode in PBS solution including different Fe^{3+}concentrations in range of [0.5 μM-120 mM].

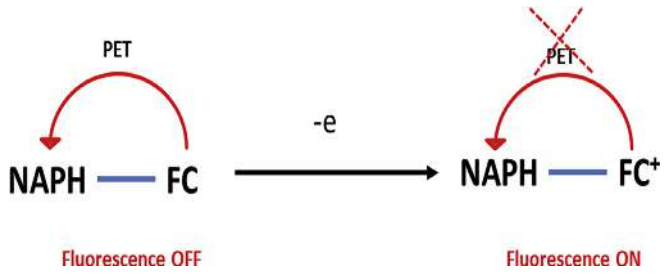

Scheme 3. The reaction involved at the (FC-NAPH) molecular level and the PET mechanism.

To determine the sensitivity of the designed sensor to the electrolyte pH, by acetate/sodium carbonate buffers, the pH of the PBS solution (including 2.0 mM Fe^{3+}) was changed from 2.0 to 13.0. The results of the CV and spectrofluorometric tests are shown in Fig. 7. The spectrofluorometric test was performed simultaneously with a CV test from the surface of the electrode samples.

As can be seen in Fig. 7a, peak potentials shifted as a function of pH. Also, with the acidification of the PBS electrolyte, the intensity of the anodic and cathodic currents of the oxidation and reduction of the (FC-NAPH) compound was reduced. The reason for this can be related to the dissolution of the existing metal ions (Mg^{2+} and Al^{3+}) in the LDHs structure under strong acidic conditions (pH < 5), which leads to instability in the molecular structure of the adsorbed $(NALD)_5$ matrix on the electrode surface. Under these conditions, desorption occurs in the adsorbed layers on the surface of the (GO/ITO/PET) electrode. Reducing the fluorescence emission (results of Fig. 7b) also confirmed this. Also, in alkaline conditions, due to the presence of hydroxyl ions in the electrolyte and the overlapping of Fe^{3+} ions in the (FC-NAPH) compound by hydroxyl ions, the intensity of the anodic and cathodic signals of the (FC-NAPH) compound decreased. The results in Fig. 7d also confirm the reduction of fluorescence emission due to the lower reduction reaction rate of the (FC-NAPH). According to the summary of the above results and Fig. 7e, the sensor showed the highest sensitivity from pH 7.0 to 8.0. This range of pH is suitable for the detection of biological species in biosensors, and in many studies, this pH range has been more efficient.

Regarding the reduction ability of DA, the back reduction of $(Fc\text{-}NDPH)^{+}$ took place when DA was added. Ten seconds after the addition of DA to the electrolyte, the voltammetric response was evaluated, the results of which are shown in Fig. 8. Also, after each CV test, the spectrofluorometric test was performed on the electrode surface, and the results are given in Fig. 9.

The results of the cyclic voltammograms and the increase in anodic signal at about −0.01 (V vs Ag/AgCl) confirm this mechanism in comparison with the approximate stagnation of the reduction peak current. According to the results of Fig. 8b, the linear response ranges in $[10^{-10}\text{-}1.5 \times 10^{-8}$ M] with a regression equation of i_{pa} (μA) = 37.98C (μM)+19.537, $r^2 = 0.966$, and a detection limit of 0.06 nM for DA was obtained.

Electro-optical sensing mechanism: Regarding Scheme 3, due to the presence of Fe^{2+} in the basic structure of the (FC-NAPH) dye, while the naphthalimide ring (fluorophore) is excited due to the electron transfer with the PET mechanism from the ferrocene side, the fluorescence emission of the resulting compound (FC-NAPH) is **OFF** [40]. Now, by adding different concentrations of Fe^{3+} to the PBS electrolyte and the oxidation of Fe^{2+} to Fe^{3+} ion in the ferrocene unit, $(Fc\text{-}Naphthalimide)^{+}$ is formed, the PET mechanism is discontinued in the structure of the dye molecule, and the fluorescence emission is turned **ON** (see Fig. 9a and Fig. 10). The linear behaviour in increasing the fluorescence emission is shown in Fig. 9b. With the addition of DA to the PBS electrolyte, a decrease in

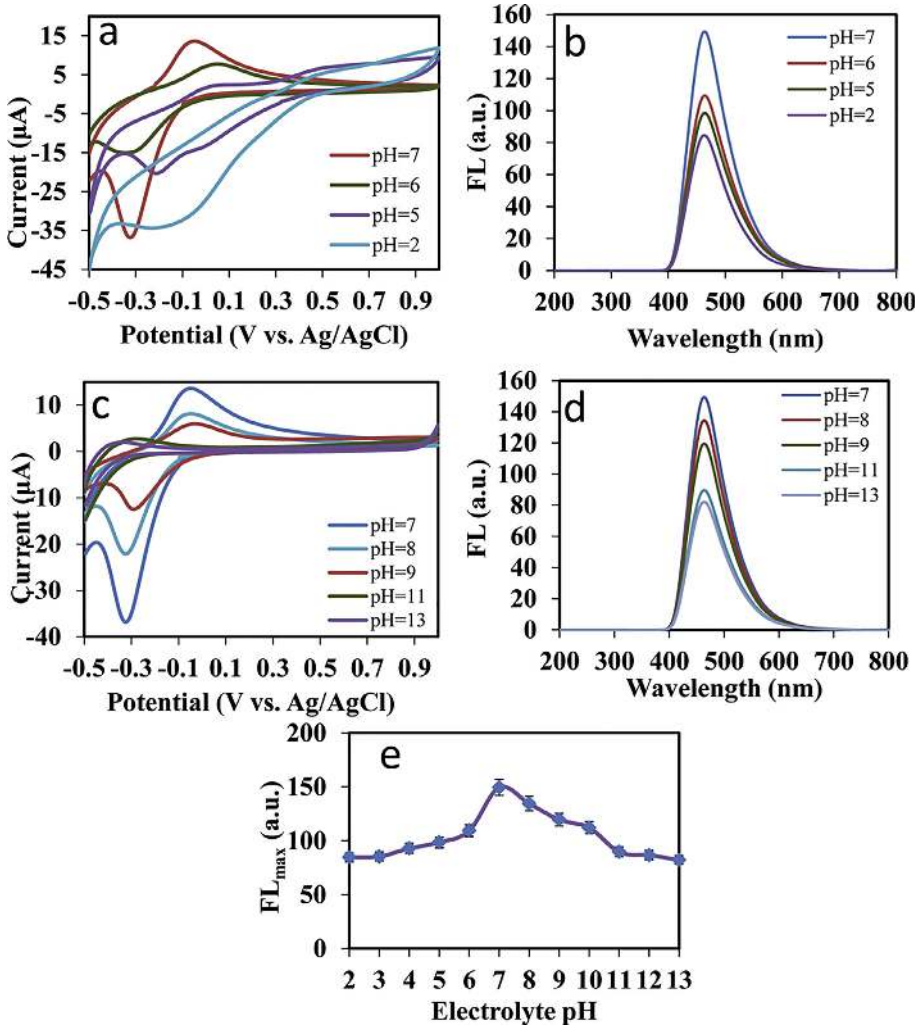

Fig. 7. (a) The cyclic voltammograms of NALD-5 electrode in PBS solution in acidic conditions including 2.0 mM Fe^{3+}, (b) the fluorescence emission changes of NALD-5 electrode in acidic conditions of PBS solution, (c) The cyclic voltammograms of NALD-5 electrode in PBS solution in alkaline conditions including 2.0 mM Fe^{3+}, (d) the fluorescence emission changes of NALD-5 electrode in alkaline conditions of PBS solution, (e) maximum fluorescence emission changes of NALD-5 electrode against electrolyte pH.

fluorescence emission is observed due to the back reduction of Fe^{3+} ions in the ferrocene unit, resulted in PET returning and fluorescence quenching (see Fig. 9a and Fig. 10). Regarding the presence of Fe^{3+} inside the electrolyte and its oxidizing role for the ferrocene in the (FC-NAPH) structure that is present on the electrode surface, the presence of an electro-active target molecule that can act as an iron ion-reducing agent in this system can affect the ferrocene anodic signal at −0.01 V (vs. Ag/AgCl).

3.4. Selective determination of DA

AA and DA coexist in the extra-cellular fluid of the central nervous system. The similar oxidation potential of these two at most solid-state electrodes is a great challenge due to their overlapping signal; therefore, the separate determination of these species is very important [64]. To evaluate the selectivity of the (NALD-5) electrode to DA, five different concentrations of DA (0.15 nM, 0.5 nM, 5 nM, 50 μM, and 100 μM), AA, and UA were prepared. All solutions were made in 0.1 M PBS at pH 7.0. After adding 2 mM Fe^{3+} to 0.1 M PBS electrolyte, various concentrations of the target were added to the electrolyte. At the same time, after adding any analyte concentration, the CV and spectrofluorimetric tests were taken from the electrode surface. The results of the anodic signal difference at about −0.01 V vs Ag/AgCl after the addition of target analytes to the electrolyte compared with that without target analytes and the ratio of the maximum fluorescence emission at 460 nm compared with the initial emission of the electrode are given in Fig. 11. Also, we used the NALD-5 to detect of DA in the presence of structural analogue mixture (AA + UA). The concentration of DA was fixed at 5 nM, while the concentration of AA and UA were ranged from 5 nM to 25 nM (Fig. 12).

According to the results, a significant difference in the anodic signal differences at about −0.01 V vs Ag/AgCl can be detected in all DA concentrations. The effect of fluorescence quenching is also evident with increasing DA concentrations relative to other target analytes. As the results show, the amount of electrochemical signal changes for DA is much higher than other targets. It can be seen from Fig. 11 that the sensitivity of the sensor to DA in the concentration range of [0.15–5 nM] is approximately 10 and 13 times higher than AA and UA, respectively. As shown in Fig. 12a and b, the NALD-5 did not show significant difference toward AA and UA than DA, even though the concentration of the structural analogues was 5 times of DA. In a study conducted by Erdogdu and Mutlu [65], they also found the same result as our research, and showed that when the concentration of AA is greater than that of DA (AA/DA>1), there is no significant difference in the anodic signal associated

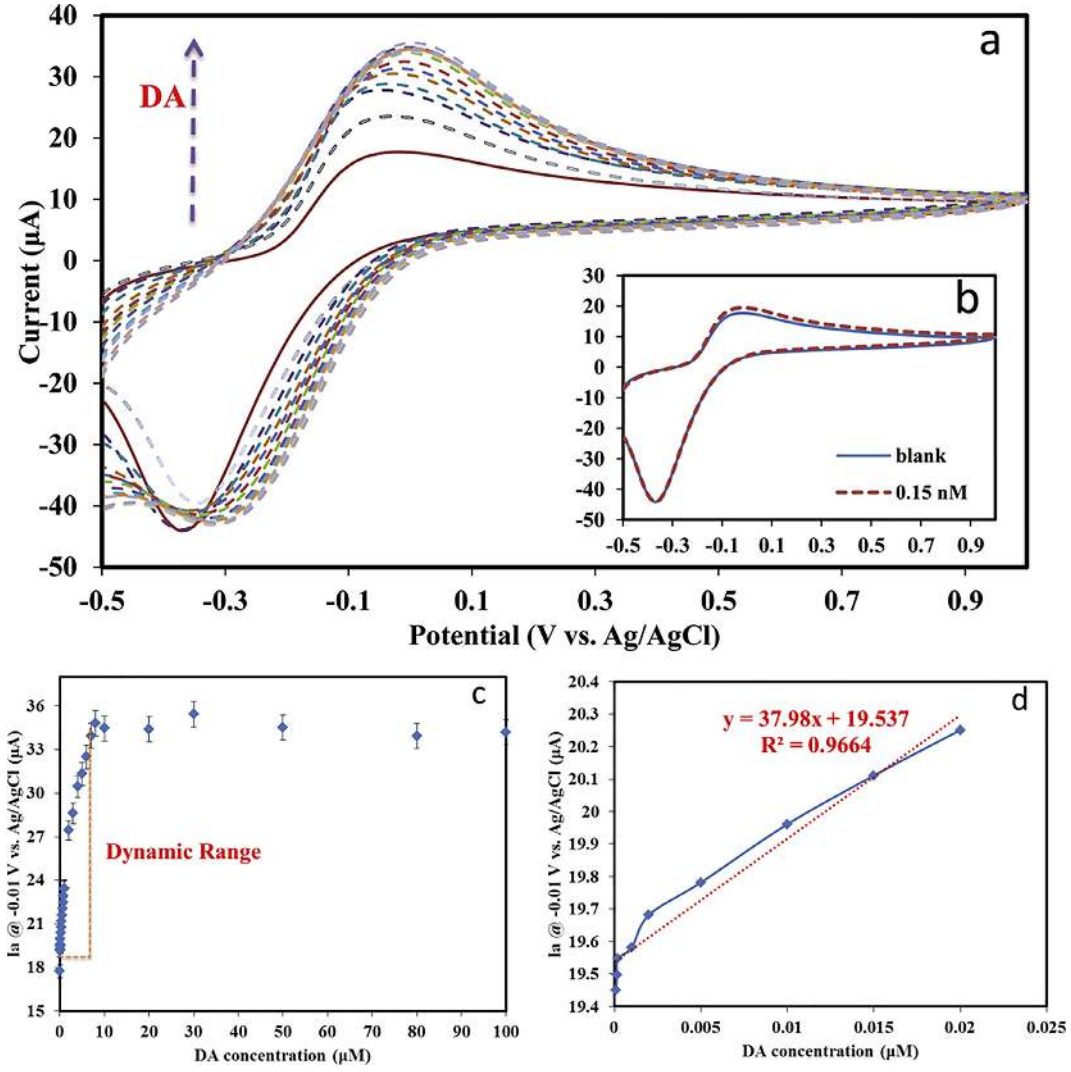

Fig. 8. (a) The cyclic voltammetric response of NALD-5 electrode after adding different concentrations of DA in PBS electrolyte including 2.0 mM Fe^{3+}, (b) electrochemical signal changes of NALD-5 electrode after adding 0.15 nM DA in PBS electrolyte including 2.0 mM Fe^{3+}, (c) anodic current changes against different concentrations of DA (from 10^{-10} to 10^{-4} M), (d) anodic current changes against different concentrations of DA (from 1.0×10^{-10} to 1.5×10^{-8} M).

with the oxidation of ascorbic acid on the surface of the solid electrode. This point could be a good measure of the selectivity of the sensor designed in the range of electroactive biomolecules in real samples. The observed changes in the anodic signal can be related to the variations in the reduction strength of different target analytes. Since the electrochemical activity (electrochemical reducing tendency) of different targets varies on this platform as oxidation catalyst [66], this sensor will be able to detect selectively. This result indicates that NALD-5 has apparent catalytic effect on the redox reaction of DA that makes the response currents increase sharply. Otherwise, the electrocatalytic oxidation effect of AA and UA can be eliminated at NALD-5. Other researchers also found the same result on solid-state modified electrodes for selective detection of DA in the presense of AA [67,68]. The results of this study showed good selectivity for a sensor designed for DA in physiological pH.

3.4.1. Analytical performance for determination of DA in the pharmaceutical sample

To test the validity of this method, the modified electrode NALD-5 was applied to determine the DA contents in real samples. Before experiments, 10 mL of 2.0 mM iron (III) sulfate hydrate solution in deionized water was added to 100 mL of 0.1 M PBS electrolyte and mixed well. This electrolyte was selected as PBS electrolyte #1. Subsequently, a CV test was performed on the modified electrode surface in PBS electrolyte #1. Following this, the DA injection solution was directly diluted with 0.1 M PBS electrolyte #1 without any other pretreatment. Table 2 shows the results of recovery tests, which were used to examine the reliability and accuracy of this method. The concentrations of DA in the injection solution are in good agreement with the labelled value (20.0 nM) with the (R.S.D.) of 2.14% for n = 6. Therefore, the modified NALD-5 electrode can be used to determine nanomolar DA levels in real samples.

Moreover, 10 replicate measurements of 0.15 nM DA on the modified electrode yielded a reproducible current and maximum fluorescence intensity with the (R.S.D.) of 2.5% and 2.3%, respectively; also, six independent modified electrodes were prepared using the same procedure and used for determination of DA (0.15 nM) with the (R.S.D.) of 1.8%, demonstrating the good repeatability and reproduction ability of the electrochemical sensor. The long-term and extremely high flexibility was investigated by measuring the current response of 0.15 nM DA after the bending test (in a cylindrical manner to a 90° angle) of the modified GO/ITO/PET electrode 90 times during one month; recovery was

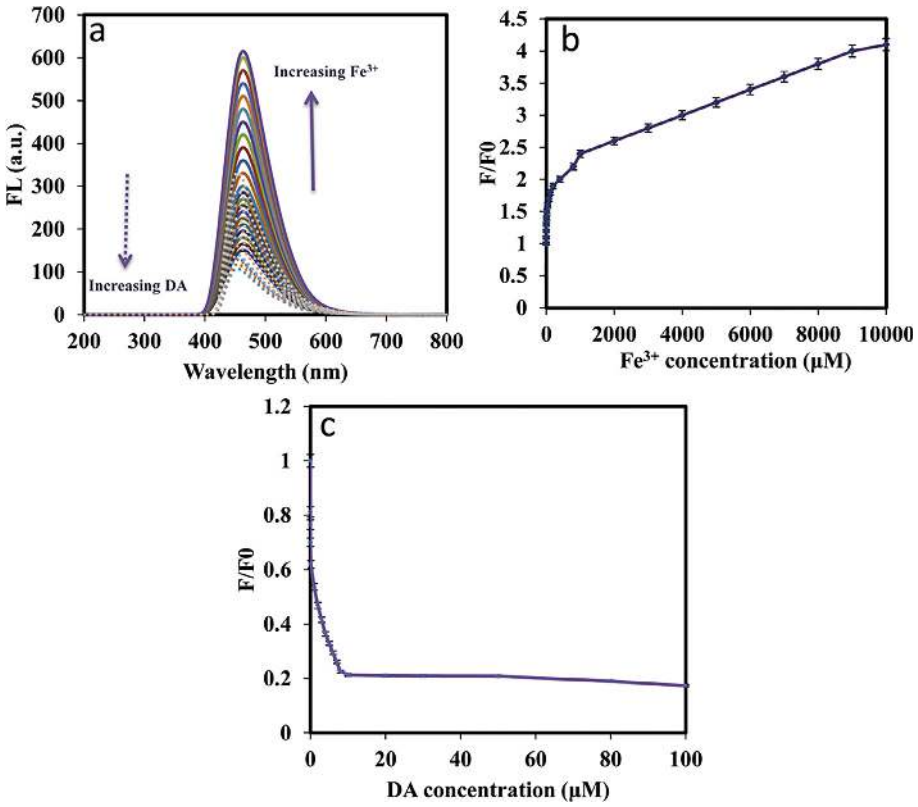

Fig. 9. (a) Fluorescence emission changes of NALD-5 electrode after adding different concentrations of Fe^{3+} and DA, (b) fluorescence emission changes of NALD-5 electrode against Fe^{3+} concentrations [0.5×10^{-6}-1×10^{-2} M], (c) fluorescence emission changes of NALD-5 electrode against DA concentrations [1.0×10^{-10}-10^{-4} M].

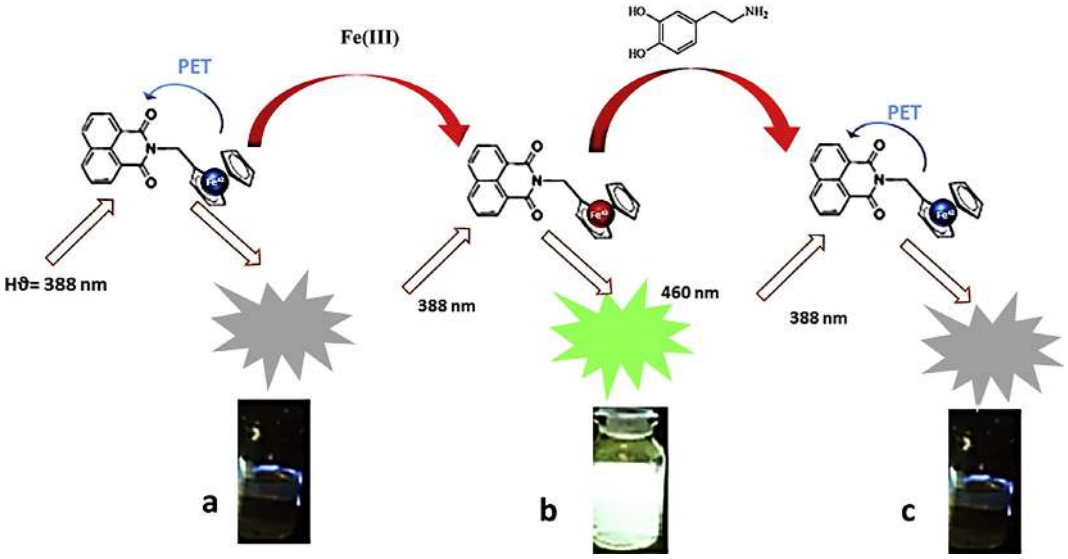

Fig. 10. Schematic illustration of fluorescence enhancement/quenching of designed sensor (a:FC-NAPH solution (1.0 g L^{-1} in DMF), b: FC-NAPH solution (1.0 g L^{-1} in DMF) including 2.0 mM Fe^{3+}, c:FC-NAPH solution (1.0 g L^{-1} in DMF) including 2.0 mM Fe^{3+} and 1.0 mM DA/all photos are taken under UV cabin with excitation wavelength of 366 nm).

96%, indicating the long-term lifetime and stability of the modified flexible electrode.

The detection limit was lower in this work than in previous works; also, the sensor designed in this study compared to other research has a simple and low-cost construction method. It also has a flexible surface and is able to detect two types of analyte (metal ion/biomolecule) in dual mode with two electrochemical and optical strategies. Also, in the molecular design of this sensor, due to the presence of several nanometric layers of GO and LDHs, a highly conductive network increases the direct electron transfer (DET) rate, which leads to the development of rapid sensing assays. In vivo monitoring is challenging because the response time for neurotransmitters is fast, rapidly released from the extracellular space, and their concentration is usually very low. Considering the

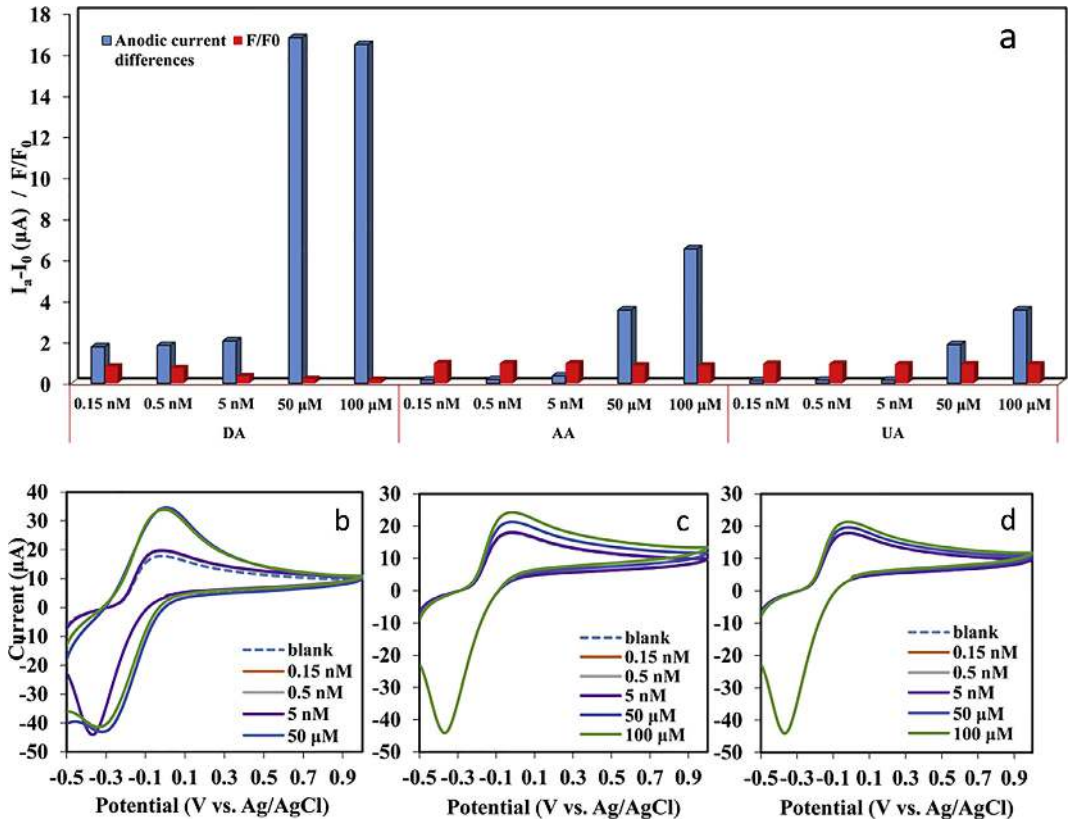

Fig. 11. (a) Selectivity illustration of NALD-5 to DA compared to other target analytes via electro/optical strategies, (b) cyclic voltammograms of NALD-5 against different concentrations of DA (0.15 nM, 0.5 nM, 5 nM, 50 μM, and 100 μM), (c) cyclic voltammograms of NALD-5 against different concentrations of AA (0.15 nM, 0.5 nM, 5 nM, 50 μM, and 100 μM), (d) cyclic voltammograms of NALD-5 against different concentrations of UA (0.15 nM, 0.5 nM, 5 nM, 50 μM, and 100 μM).

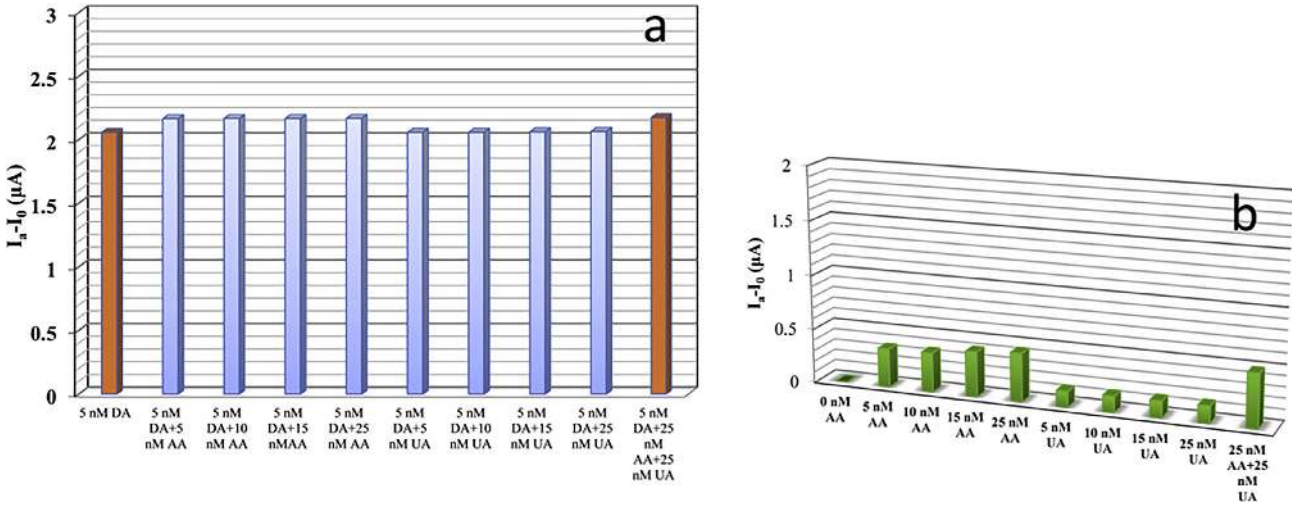

Fig. 12. (a) Comparison of the anodic signal differences of NALD-5 toward DA in the presence of (AA + UA) mixture, (b) anodic signal differences of NALD-5 toward AA and UA in different concentrations [5 nM-25 nM].

features of the new electrochemical sensor introduced in this study, this sensor can also be effective in detecting the amount of dopamine in biological real samples whose tests are being investigated in our Research Group.

4. Conclusion

In this study, a novel flexible ITO/PET-based electrochemical sensor was designed and constructed. The sheet resistance was reduced by about 24 Ω, due to the increase in the electrical conductivity of the electrode surface with the GO electrophoretically deposited (a multi-nanometer thickness) on the electrode surface. The results of this study showed that the LbL assembly of LDH nanoplatelets along with the electro-active naphthalimide dye molecules (FC-NAPH), up to five cycles, formed a conductive matrix network with uniform morphology and topology. The minimum

Table 2
Results of DA detection in DA hydrochloride injection (n = 6).

Electrode/n	Added	Detected	Recovery (%)	RSD (%)
NALD-5/1	20.0 nM	20.23 nM	101.1	2.14
NALD-5/2	20.0 nM	20.96 nM	104.8	
NALD-5/3	20.0 nM	20.75 nM	103.7	
NALD-5/4	20.0 nM	19.94 nM	99.7	
NALD-5/5	20.0 nM	19.96 nM	99.8	
NALD-5/6	20.0 nM	20.11 nM	100.5	
NALD-5/1	20.0 μM	20.85 μM	104.2	3.89
NALD-5/2	20.0 μM	20.95 μM	104.7	
NALD-5/3	20.0 μM	20.77 μM	103.8	
NALD-5/4	20.0 μM	19.25 μM	96.2	
NALD-5/5	20.0 μM	20.98 μM	104.9	
NALD-5/6	20.0 μM	19.55 μM	97.7	

sheet resistance with high electrocatalytic function was obtained in the fifth cycle of the LbL assembly. This molecular design resulted in a significant increase in fluorescence emission of the electro-active dye in the sensor's bed containing LDH nanoplatelets and the elimination of the effect of GO quenching. By LbL assembly of the $(NALDs)_5$ matrix grid, a sensitive sensor was obtained for the dual detection of Fe^{3+}/DA. Due to the presence of highly sensitive fluorescent electro-active naphthalimide dye adsorbed on the surface of electrode tendency for electrochemical reactions of (FC-NAPH) to $(FC\text{-}NAPH)^+$, the device dually senses well electro- and optically the Fe^{3+} ions. With electrochemical/optical changes, Fe^{3+} on the surface of this electrode was detected (LOD = 0.03 μM). The back reduction of $(FC\text{-}NAPH)^+$ with DA resulted in high sensitivity toward DA sensing. In the molecular design of the solid structure of this sensor (in terms of electrochemical/optical changes), the (OFF/ON/OFF) system was created, so that the fluorescence emission decreased in the presence of DA molecules. In this electrochemical sensor, both electrochemical and optical methods were detected with high DA sensitivity; in a CV-based electrochemical method, the detection limit of 0.06 nM with a linear range [10^{-10}-1.5×10^{-8} M] was obtained. The results of this study showed well that the (NALD-5) modified electrode could be very effective in detecting nanomolar DA levels in real pharmaceutical samples of dopamine hydrochloride injections.

Acknowledgements

We would like to appreciate the Center of Excellence for Color Science and Technology (CECST), Institute for Color Science and Technology, Tehran-Iran for providing us a good environment and facilities to complete this project.

References

[1] M. Hosseini, M.R. Karimipur, P. Norouzi, M.R. Moghaddam, F. Faridbod, M.R. Ganjali, J. Shamsi, Enhanced solid-state electrochemiluminescence of $Ru(bpy)_3^{2+}$ with nano-CeO_2 modified carbon paste electrode and its application in tramadol determination, Anal. Methods 7 (2015) 1936.
[2] N. Weidan, Q. Zhengyi, C. Xueqian, S. Xingguang, A turn-on fluorescent probe for sensitive detection of sulfide anions and ascorbic acid by using sulfanilic acid and glutathione functionalized graphene quantum dots, Sensor. Actuator. B Chem. 256 (2018), 256 48.
[3] R. Ke, X. Zhang, L. Wang, C. Zhang, S.C. Mao, H. Niu, J. Song, B. Jin, Y. Tian, Electrochemiluminescence sensor based on Graphene Oxide/Polypyrrole/CdSe nanocomposites, J. Alloy. Comp. 622 (2015) 1027.
[4] K. Jayakumar, C. María Belén, V. Dharuman, J. Huangxian, S.D. Ramendra, W. Yangping, Correction: one-step coelectrodeposition-assisted layer-by-layer assembly of gold nanoparticles and reduced graphene oxide and its self-healing three-dimensional nanohybrid for an ultrasensitive DNA sensor, Nanoscale 10 (2018) 1196.
[5] G. Guangwei, L. Jie, G. Zaochuan, C. Shaojun, C. Shiguo, Y. Haipeng, Self-assembling of electrochemical glucose biosensor with bacteriostatic materials via layer-by-layer method, J. Electrochem. Soc. 164 (2017) 189.
[6] S. Run-Min, L. Zhan-Hong, W. Peng-Ju, Z. Xue-Ling, C. Cheng, Z. Zhi-Gang, Flexible hydrogen peroxide sensors based on platinum modified free-standing reduced graphene oxide Paper, Appl. Sci. 8 (2018) 848.
[7] T. Yuan, L. Pu, Q. Huang, H. Zhang, X. Li, H. Yang, An effective methanol-blocking membrane modified with graphene oxide nanosheets for passive direct methanol fuel cells, Electrochim. Acta 117 (2014) 393.
[8] B. Si, E. Song, Recent advances in the tetection of neurotransmitters, Chemosensors 6 (2018) 1.
[9] J. Du, R. Yue, F. Ren, Z. Yao, F. Jiang, P. Yang, Y. Du, Novel graphene flowers modified carbon fibers for simultaneous determination of ascorbic acid, dopamine and uric acid, Biosens. Bioelectron. 53 (2014) 220.
[10] C. Wang, J. Du, H. Wang, C. Zou, F. Jiang, P. Yang, Y. Du, A facile electrochemical sensor based on reduced graphene oxide and Au nanoplates modified glassy carbon electrode for simultaneous detection of ascorbic acid, dopamine and uric acid, Sensor. Actuator. B Chem. 204 (2014) 302.
[11] Q. Huang, H. Zhang, S. Hu, F. Li, W. Weng, J. Chen, Q. Wang, Y. He, W. Zhang, X. Bao, A sensitive and reliable dopamine biosensor was developed based on the Au@carbon dots-chitosan composite film, Biosens. Bioelectron. 52 (2014) 277.
[12] Y.J. Yang, W. Li, CTAB functionalized graphene oxide/multiwalled carbon nanotube composite modified electrode for the simultaneous determination of ascorbic acid, dopamine, uric acid and nitrite, Biosens. Bioelectron. 56 (2014) 300.
[13] D. Yuan, S. Chen, R. Yuan, J. Zhang, X. Liu, An ECL sensor for dopamine using reduced graphene oxide/multiwall carbon nanotubes/gold nanoparticles, Sensor. Actuator. B Chem. 191 (2014) 415.
[14] A. Numan, M.M. Shahid, F.S. Omar, K. Ramesh, S. Ramesh, Facile fabrication of cobalt oxide nanograin-decorated reduced graphene oxide composite as ultrasensitive platform for dopamine detection, Sensor. Actuator. B Chem. 238 (2017) 1043.
[15] W. Al-Graiti, Z. Yue, J. Foroughi, X.F. Huang, G. Wallace, R. Baughman, J. Chen, Probe sensor using nanostructured multi-walled carbon nanotube yarn for selective and sensitive detection of dopamine, Sensors 17 (2017) 884.
[16] S. Kruss, M.P. Landry, E. Vander Ende, B.M.A. Lima, N.F. Reuel, J. Zhang, J. Nelson, B. Mu, A. Hilmer, M. Strano, Neurotransmitter detection using corona phase molecular recognition on fluorescent single-walled carbon nanotube sensors, J. Am. Chem. Soc. 136 (2014) 713.
[17] S. Kruss, D.P. Salem, L. Vukovĭc, B. Lima, E.V. Ende, E.S. Boyden, M.S. Strano, High-resolution imaging of cellular dopamine efflux using a fluorescent nanosensor array, Proc. Natl. Acad. Sci. U.S.A. 114 (2017) 1789.
[18] S. Baluta, J. Cabaj, K. Malecha, Neurotransmitters detection using a fluorescence-based sensor with graphene quantum dots, Opt. Appl. 47 (2017).
[19] A. Gupta, C.K. Nandi, PC12 live cell ultrasensitive neurotransmitter signaling using high quantum yield sulphur doped carbon dots and its extracellular Ca^{2+} ion dependence, Sensor. Actuator. B Chem. 245 (2017) 137.
[20] T.T.-C. Tseng, H.G. Monbouquette, Fabrication of implantable, enzyme-immobilized glutamate sensors for the monitoring of glutamate concentration changes in vitro and in vivo, J. Electroanal. Chem. 682 (2012) 141.
[21] Z. Rui, W. Huang, Y. Chen, K. Zhang, Y. Cao, J. Tu, Facile synthesis of graphene/polypyrrole 3D composite for a high-sensitivity non-enzymatic dopamine detection, J. Appl. Polym. Sci. 134 (2017).
[22] X. Li, X. Lu, X. Kan, 3D electrochemical sensor based on poly(hydroquinone)/gold nanoparticles/nickel foam for dopamine sensitive detection, J. Electroanal. Chem. 799 (2017) 451.
[23] E.A. Khudaish, F. Al-Nofli, J.A. Rather, M. Al-Hinaai, K. Laxman, H.H. Kyaw, S. Al-Harthy, Sensitive and selective dopamine sensor based on novel conjugated polymer decorated with gold nanoparticles, J. Electroanal. Chem. 761 (2016) 80.
[24] J. Li, J. Zhao, X. Wei, A sensitive and selective sensor for dopamine determination based on a molecularly imprinted electropolymer of o-aminophenol, Sensor. Actuator. B Chem. 140 (2009) 663.
[25] T. Qian, C. Yu, X. Zhou, P. Ma, S. Wu, L. Xu, J. Shen, Ultrasensitive dopamine sensor based on novel molecularly imprinted polypyrrole coated carbon nanotubes, Biosens. Bioelectron. 58 (2014) 237.
[26] Y. Teng, F. Liu, X. Kan, Voltammetric dopamine sensor based on three-dimensional electrosynthesized molecularly imprinted polymers and polypyrrole nanowires, Microchim. Acta 184 (2017) 2515.
[27] B. Li, Y. Zhou, W. Wu, M. Liu, S. Mei, Y. Zhou, T. Jing, Highly selective and sensitive determination of dopamine by the novel molecularly imprinted poly(nicotinamide)/CuO nanoparticles modified electrode, Biosens. Bioelectron. 67 (2015) 121.
[28] Y. Xu, X. Hun, F. Liu, X. Wen, X. Luo, Aptamer biosensor for dopamine based on a gold electrode modified with carbon nanoparticles and thionine labeled gold nanoparticles as probe, Microchim. Acta 182 (2015) 1797.
[29] A. Azadbakht, M. Roushani, A.R. Abbasi, Z. Derikvand, Design and characterization of electrochemical dopamine-aptamer as convenient and integrated sensing platform, Anal. Biochem. 507 (2016) 47.
[30] L. Liu, N. Xia, J.-J. Meng, B.-B. Zhou, S.-J. Li, An electrochemical aptasensor for sensitive and selective detection of dopamine based on signal amplification of electrochemical-chemical redox cycling, J. Electroanal. Chem. 775 (2016) 58.
[31] S. Bahrami, A.R. Abbasi, M. Roushani, Z. Derikvand, A. Azadbakht, An electrochemical dopamine aptasensor incorporating silver nanoparticle, functionalized carbon nanotubes and graphene oxide for signal amplification, Talanta 159 (2016) 307.
[32] W. Wang, W. Wang, J.J. Davis, X. Luo, Ultrasensitive and selective voltammetric aptasensor for dopamine based on a conducting polymer

nanocomposite doped with graphene oxide, Microchim. Acta 182 (2015) 1123.
[33] D.R. Raj, S. Prasanth, T.V. Vineeshkumar, C. Sudarsanakumar, Surface plasmon resonance based fiber optic dopamine sensor using green synthesized silver nanoparticles, Sensor. Actuator. B Chem. 224 (2016) 600.
[34] S. Jafarinejad, M. Ghazi-Khansari, F. Ghasemi, P. Sasanpour, M.R. Hormozi-Nezhad, Colorimetric fingerprints of gold nanorods for discriminating catecholamine neurotransmitters in urine samples, Sci. Rep. 7 (2017) 8266.
[35] M.H. Kim, H. Yoon, S.H. Choi, F. Zhao, J. Kim, K.D. Song, U. Lee, Miniaturized and wireless optical neurotransmitter sensor for real-time monitoring of dopamine in the brain, Sensors 16 (2016) 1894.
[36] K. Jackowska, P. Krysinski, New trends in the electrochemical sensing of dopamine, Bioanal. Chem. 405 (2013) 3753.
[37] G.W. She, X. Huang, L.L. Jin, X.P. Qi, L.X. Mu, W.S. Shi, SnO_2 nanoparticle-coated ZnO nanotube arrays for high-performance electrochemical sensors, Small 10 (2014) 4685.
[38] B. Nagendra, K. Mohan, E.B. Gowd, Polypropylene/layered double hydroxide (LDH) nanocomposites: influence of LDH particle size on the crystallization behavior of polypropylene, ACS Appl. Mater. Interfaces 7 (2015) 12399.
[39] M.H. Parvin, E. Azizi, J. Arjomandi, J.L. Lee, Highly sensitive and selective electrochemical sensor for detection of vitamin B12 using an Au/PPy/FMNPs@TD-modified electrode, Sensor. Actuator. B Chem. 261 (2018) 335.
[40] L. Wang, W. Wang, X. Wang, X. Feng, X. Ye, J. Fu, Small-sized Mg–Al LDH nanosheets supported on silica aerogel with large pore channels: textural properties and basic catalytic performance after activation, Nanomaterials 8 (2018) 113.
[41] Y. Zhou, D. Yan, M. Wei, A 2D quantum dot-based electrochemiluminescence film sensor towards reversible temperature-sensitive response and nitrite detection, J. Mater. Chem. C 3 (2015) 10099.
[42] C. Hobbs, S. Jaskanie, E.K. McCarthy, C. Downing, K. Opelt, K. Güth, A. Shmeliov, M.C.D. Mourad, M C D, K. Mandel, V. Nicolosi, Structural transformation of layered double hydroxides: an in situ TEM analysis, npj 2D Materials and Applications 4 (2018), https://doi.org/10.1038/s41699-018-0054-6.
[43] E.F. Grosu, D. Simiuc, R. Froidevaux, Layered double hydroxides nanomaterials in biomedicine and (bio) sensing design, Biomed J Sci & Tech Res. 2 (2018) 1.
[44] C. Taviot-Gueho, V. Prevot, C. Forano, G. Renaudin, C. Mousty, F. Leroux, Tailoring hybrid layered double hydroxides for the development of innovative applications, Adv. Funct. Mater. 28 (2017), 1703868.
[45] X. Minxuan, Q. Junjie, L. Feng, Z. Yue, Highly stretchable strain sensors with reduced graphene oxide sensing liquids for wearable electronics, Nanoscale 10 (2018) 5264.
[46] M.K. Bhatt, C. Rani, A. Kapoor, P. Kumar, S. Sandeep, S. Kumar, R. Singh, C.C. Tripathi, A facile approach to fabricate graphene based piezoresistive strain sensor on paper substrate, Indian J. Pure Appl. Phys. 56 (2018) 361.
[47] P.O. Huang, J. Liu, DNA-length-dependent fluorescence signaling on graphene oxide surface, Small 8 (2012) 977.
[48] N. Anindya, M. Arkadeep, C.M. Subhas, Graphene and its sensor-based applications: a review, Sens Actuators A Phys 270 (2018) 177.
[49] W. Liu, X. Zhang, G. Wei, Z. Su, Reduced graphene oxide-based double network polymeric hydrogels for pressure and temperature Sensing, Sensors 18 (2018) 3162.
[50] S.L. Esfahani, S. Rouhani, Z. Ranjbar, Optimization the electrophoretic deposition fabrication of graphene-based electrode to consider electro-optical applications, Surf. Interfac. 9 (2017) 218.
[51] J.C. Spiteri, J.S. Schembri, D.C. Magri, A naphthalimide-based 'Pourbaix sensor': a redox and pH driven AND logic gate with photoinduced electron transfer and internal charge transfer mechanisms, New J. Chem. 39 (2015) 3349.
[52] E. Alibakhshi, E. Ghasemi, M. Mahdavian, B. Ramezanzadeh, S. Farashi, Active corrosion protection of Mg-Al-PO43− LDH nanoparticle in silane primer coated with epoxy on mild steel, J. Taiwan Inst. Chem. Eng. 75 (2017) 248.
[53] W. Gao, L.B. Alemany, L.J. Ci, P.M. Ajayan, New insights into the structure and reduction of graphite oxide, Nat. Chem. 1 (2009) 403.
[54] M.N. Sepehr, T.J. Al-Musawi, E. Ghahramani, H. Kazemian, M. Zarrabi, Adsorption performance of magnesium/aluminum layered double hydroxide nanoparticles for metronidazole from aqueous solution, Arab J Chem 10 (2017) 611.
[55] M. Liu, G. Lv, L. Mei, Y. Wei, J. Liu, Z. Li, L. Liao, Fabrication of AO/LDH fluorescence composite and its detection of Hg^{2+} in water, Sci. Rep. 7 (2017) 13414.
[56] Y. Zhang, J.R.G. Evans, Alignment of layered double hydroxide platelets, Colloid. Surface. Physicochem. Eng. Aspect. 408 (2012) 71.
[57] W.G. Hu, D.J. Sun, C.G. Zhang, Y.L. Su, Studies on zero point of charge and permanent charge density of Mg− Fe hydrotalcite-like compounds, Langmuir 17 (2001) 1885.
[58] T. Forster, Delocalized Excitation and Excitation Transfer, Academic Press, New York, 1965, p. 93.
[59] A. Viehbeck, M.J. Goldberg, C.A. Kovac, Electrochemical properties of polyimides and related imide compounds, J. Electrochem. Soc. 137 (1990) 1460.
[60] M.E. Ghica, C.M.A. Brett, Development of a carbon film electrode ferrocene-mediated glucose biosensor, Anal. Lett. 38 (2005) 907.
[61] H. Yaghoubian, H. Karimi-Maleh, M.A. Khalilzadeh, F. Karimi, Electrocatalytic oxidation of levodopa at a ferrocene modified carbon nanotube paste electrode, Int. J. Electrochem. Sci. 4 (2009) 993.
[62] G.K. Jayaprakash, B.E. Kumara Swamy, N. Casillas, R.F. Moreno, Analytical fukui and cyclic voltammetric studies on ferrocene modified carbon electrodes and effect of Triton X-100 by immobilization method, Electrochim. Acta 258 (2017) 1025.
[63] J.B. Raoof, R. Ojani, M. Kolbadinezhad, Voltammetric sensor for glutathione determination based on ferrocene-modified carbon paste electrode, J. Solid State Electrochem. 13 (2008) 1411.
[64] S.S. Shankar, R.M. Shereema, G.R.D. Prabhu, T.P. Rao, B.E. Kumara Swamy, Electrochemical detection of dopamine in presence of serotonin and ascorbic acid at tetraoctyl ammonium bromide modified carbon paste electrode: a voltammetric study, J. Biosens. Bioelectron. 6 (2015) 2.
[65] G. Erdoğdu, M.M. Mutlu, Selective detection of dopamine in the presence of ascorbic acid at poly (m-aminobenzene sulfonic acid), Am. J. Anal. Chem. 2 (2011) 582.
[66] Q. Chen, S. Ai, Q. Ma, H. Yin, Selective determination of dopamine in the presence of ascorbic acid using ferrocenyl-tethered PAMAM dendrimers modified glassy carbon electrode, J. Appl. Electrochem. 40 (2010) 1379.
[67] T. Skeika, C.R. Zuconelli, S.T. Fujiwara, C.A. Pessoa, Preparation and electrochemical characterization of a carbon ceramic electrode modified with ferrocenecarboxylic acid, Sensors 11 (2011) 1361.
[68] Y. Xiao, C. Guo, C.M. Li, Y. Li, J. Zhang, R. Xue, S. Zhang, Highly sensitive and selective method to detect dopamine in the presence of ascorbic acid by a new polymeric composite film, Anal. Biochem. 371 (2007) 229.